

Trends in the Local Hadley and Local Walker Circulations

Juliane Schwendike¹, Gareth J. Berry¹, Michael J. Reeder^{1,2}, Christian

Jakob^{1,2}, Pallavi Govekar^{1,3}, and Richard Wardle⁴

Gareth J. Berry, (gareth.berry@monash.edu.au)

Pallavi Govekar, (pallavi.govekar@unimelb.edu.au)

Christian Jakob, (christian.jakob@monash.edu.au)

Michael J. Reeder, (michael.reeder@monash.edu.au)

Juliane Schwendike, (juliane.schwendike@monash.edu.au)

Richard M. Wardle, (r.wardle@bom.gov.au)

¹School of Earth, Atmosphere and
Environment, Monash University, Victoria
3800, Australia.

²ARC Centre of Excellence for Climate
System Science, Monash University,
Victoria 3800, Australia.

³School of Earth Sciences, Melbourne
University, Victoria 3010, Australia.

⁴Bureau of Meteorology, 69 Ann St.,
Brisbane, Queensland 4000, Australia.

Abstract. It is widely accepted that the Hadley circulation is widening and that the Walker circulation is weakening. Here, we investigate changes in the local Hadley and Walker circulations by decomposing the vertical mass flux into a zonal and meridional component, then computing their linear trends between 1979 and 2009. This study emphasizes the regional differences in changes in the local Hadley and Walker circulations over a 31-year period. For example, the local Hadley circulation has shifted southward over Africa, the Maritime Continent as well as the western and central Pacific by about one degree. Over the Americas and the Atlantic the local Hadley circulation has strengthened by about 1-5%. The zonal component of the vertical mass flux has increased by about 10-20% in the tropics over all continents and decreased over the adjacent oceans by about 10-20%. Although the local Walker circulations in the Indian Ocean and the Atlantic have weakened, the circulation in the Pacific has shown only small changes (by about 1-2%). The local Walker circulations in all ocean basins have shifted westwards by about 1-2° on average.

1. Introduction

The Hadley and Walker circulations are the largest overturning circulations in the atmosphere and they cover about one third of the globe. The Hadley circulation is a large-scale meridional overturning circulation, which shows a strong seasonal variability and is driven by latitudinal heating gradients. The Walker circulation is a large-scale zonal overturning circulation over the Pacific, the interannual variability of which is linked the El Niño Southern Oscillation (ENSO). Changes in both circulations are associated with changes in precipitation.

Although there is agreement in the literature that the tropics have expanded [e.g. *Seidel and Randel, 2007; Lu et al., 2007; Hu and Fu, 2007; Seidel et al., 2008; Johanson and Fu, 2009; Fu and Lin, 2011; Liu et al., 2012; Nguyen et al., 2013; Quan et al., 2014*], there is disagreement on the rate of this expansion. The trends for the northern and southern cell are different and range from 0.1 to over 1.0° latitude per decade [*Lucas et al., 2013*].

These trends in the Hadley circulation have been based on changes in the tropopause height [e.g. *Seidel and Randel, 2007; Lu et al., 2007; Davis and Rosenlof, 2012*], the mass stream function, or by changes in the position of the jet stream [e.g. *Davis and Rosenlof, 2012; Davis and Birner, 2013*] in reanalyses data. Additionally, trends have been based on satellite-based methodologies [e.g. *Fu et al., 2006; Hu and Fu, 2007; Seidel et al., 2008; Johanson and Fu, 2009; Fu and Lin, 2011; Stachnik and Schumacher, 2011; Allen et al., 2012; Nguyen et al., 2013; Hu and Fu, 2013*]. A recent comparison of model simulations and reanalyses by *Quan et al. [2014]* revealed a tropical expansion rate of 0.1–0.2° latitude

per decade, which is thought to be more realistic than an expansion rate of 1.0° latitude per decade.

The expansion of the Hadley circulation has been examined in many modeling studies using, for instance, paleoclimate, 20th century and climate change scenarios. The Coupled Model Intercomparison Project phase 3 models shows a poleward expansion of the Hadley circulation by about $1 - 2^\circ$ over the 21st century and a decrease in the intensity of both the Hadley and Walker circulations due to increased greenhouse gas concentrations [e.g. *Lu et al.*, 2007; *Chen et al.*, 2002; *Held and Soden*, 2006; *Gastineau et al.*, 2008]. *Lucas et al.* [2013], however, points out that there is no consensus on the dynamical mechanism behind the tropical expansion.

Trends in the Walker circulation under different climate scenarios mainly show a weakening [*Tanaka et al.*, 2004; *Vecchi et al.*, 2006; *Vecchi and Soden*, 2007; *Deser and Phillips*, 2009; *Gastineau et al.*, 2009; *DiNezio et al.*, 2013; *Bayr et al.*, 2014]. The weakening of the large-scale tropical circulation leads to a reduced transport of water vapor from the boundary layer to the free atmosphere [*Held and Soden*, 2006], thereby affecting the global water cycle. *Bayr et al.* [2014] found recently that the Walker circulation in the Pacific is also shifting to the west.

Few studies have examined the regional or local Hadley circulations, two that have are *Goswami et al.* [1999] and *Gedney and Valdes* [2000]. However, there is a need to understand how these circulations change locally as those regional changes are directly linked to the local precipitation and hence linked to the potential societal impacts.

Although there is an accepted way of portraying the Hadley circulation, based on the zonally averaged mass stream function [e.g. *Hartmann*, 1994], there is no similar standard

way of portraying the Walker circulation. The Walker circulation is usually thought of as the meridionally averaged circulation, and this definition is often confined to the tropical Pacific Ocean [e.g. *Julian and Chervin, 1978; Vecchi et al., 2006; Power and Smith, 2007; Tokinaga et al., 2012*]. But by taking the meridional average over a limited domain large parts of the local Hadley circulation are attributed to the Walker circulation [*Schwendike et al., 2014*]. Unless the separation into a local Hadley and local Walker circulation is done carefully, the two orthogonal overturning circulations may not sum to the original three-dimensional circulation. This is a problem, particularly when attributing changes in the circulation to either the Hadley or the Walker circulation.

One way of describing the local Hadley and local Walker circulations is by using a variation of the ψ -vector method developed by *Keyser et al. [1989]*. This method uniquely and objectively partitions the divergent (irrotational) part of the three-dimensional flow into a pair of orthogonal two-dimensional circulations [*Schwendike et al., 2014*]. Based on this method the present paper investigates how the local Hadley and local Walker circulations have changed between 1979 and 2009 in four reanalyses data sets.

The remainder of the paper is structured as follows. The data and methodology used in this study are outlined in Section 2. The annual and seasonal distribution of the mass flux, diabatic heating and rainfall as well as their respective linear trends are discussed in Section 3. Section 4 examines the local Hadley and Walker circulations and their trends. The meridionally and zonally averaged mass flux is discussed in Sections 5 and 6, respectively. The relationship between the trends in both circulations and ENSO is discussed in Section 7. The key conclusions are summarised in Section 8.

2. Data and method

A version of the ψ -vector method, originally developed by *Keyser et al.* [1989], is used to decompose the tropical atmosphere into a pair of orthogonal overturning circulations which can be thought of as the local Hadley and local Walker circulations (for details see *Schwendike et al.* [2014]).

The vector stream function $\boldsymbol{\psi}$ is defined as

$$\nabla_p \cdot \boldsymbol{\psi} = -\nabla_p^2 \mu = \omega, \quad (1)$$

where μ is a potential function, ∇_p is the gradient operator in isobaric coordinates, and ω is the vertical motion. The divergent wind can be written in terms of the velocity streamfunction as

$$\mathbf{u}_{div} = (u_\lambda, u_\phi) = -\frac{\partial \boldsymbol{\psi}}{\partial p} = -\left(\frac{\partial \psi_\lambda}{\partial p}, \frac{\partial \psi_\phi}{\partial p}\right), \quad (2)$$

where u_λ and u_ϕ are the zonal and meridional components of the divergent part of the wind and ψ_λ and ψ_ϕ are the components of $\boldsymbol{\psi}$ in the zonal and meridional directions respectively. The vertical motion can be partitioned uniquely into the zonal and meridional planes as

$$\omega_\lambda \cos\phi = \frac{1}{a} \frac{\partial \psi_\lambda}{\partial \lambda} = \frac{1}{a^2 \cos\phi} \frac{\partial^2 \mu}{\partial \lambda^2}, \quad (3)$$

$$\omega_\phi \cos\phi = \frac{1}{a} \frac{\partial}{\partial \phi} (\psi_\phi \cos\phi) = \frac{1}{a^2} \frac{\partial}{\partial \phi} \left(\cos\phi \frac{\partial \mu}{\partial \phi} \right), \quad (4)$$

where a is the radius of the Earth. The vertical motion is the sum of the vertical motion partitioned in the two orthogonal directions $\omega = \omega_\lambda + \omega_\phi$. The upward mass fluxes associated with the zonal and meridional parts of the circulation are

$$m_\lambda = -\omega_\lambda \cos\phi/g \quad \text{and} \quad m_\phi = -\omega_\phi \cos\phi/g \quad (5)$$

respectively, where g is the gravitational acceleration.

The meridional overturning circulation at a point or in a plane is referred to as the *local Hadley circulation*, and the zonal overturning circulation at a point or in a plane is referred to as the *local Walker circulation*. Both circulations satisfy continuity independently. In the present study the local Hadley circulation is portrayed by the stream function ψ_ϕ , the vertical mass flux m_ϕ and the divergent part of the circulation in the meridional plane (u_ϕ, ω_ϕ) . Likewise, the local Walker circulation is portrayed by the stream function ψ_λ , the vertical mass flux m_λ and the divergent circulation in the zonal plane $(u_\lambda, \omega_\lambda)$.

Our version of the ψ -vector method is applied to four reanalyses in the period between 1979-2009: (i) The European Centre for Medium range Weather Forecasts (ECMWF) ERA-Interim (ERA-Interim) [Simmons et al., 2011; Dee et al., 2011], (ii) the National Centers for Environmental Prediction-Department of Energy reanalysis 2 data set (NCEP2) [Kistler et al., 2001], (iii) the NASA Modern Era Retrospective analysis for Research and Applications (MERRA) [Rienecker et al., 2011], and (iv) the Japanese Meteorological Agency 25 year reanalysis and climate data assimilation system (JRA) [Onogi et al., 2007]. Each data set is interpolated to a common $2.5 \times 2.5^\circ$ horizontal grid for consistency.

The diabatic heating rate is calculated from the ERA-Interim data as the residual from the thermodynamic equation in pressure coordinates:

$$\frac{\dot{H}}{\pi c_p} = \frac{\partial \theta}{\partial t} - u \frac{\partial \theta}{\partial x} - v \frac{\partial \theta}{\partial y} - \omega \frac{\partial \theta}{\partial p}. \quad (6)$$

Here θ is the potential temperature, \dot{H} is the diabatic heating rate per unit mass, $\pi = (p/p_0)^{R/c_p}$ is the Exner function, p_0 is the reference pressure of 1000 hPa, u and v are the components of the horizontal wind, R is the gas constant for dry air, and c_p is the specific heat of dry air at constant pressure.

3. Mass flux, diabatic heating and rainfall

The annual average of the total mass flux, which is the sum of the zonal and meridional mass flux, at 500 hPa averaged over all four reanalyses is shown in Fig. 1a. To quantify how the four reanalyses differ from each other the difference between the maximum and the minimum value at each grid point is plotted (Fig. 1b). The differences between the reanalyses are largest in the tropics, especially in the north of South America, the Maritime Continent, central Africa, over the Andes and the Himalayas. Nevertheless, the regions of upward mass flux largely coincide with the regions of precipitation (Fig. 1c). Even though the individual reanalyses vary their mean appears to give a realistic picture of the annual precipitation. The same conclusion holds for the seasonal means (not shown). The annually averaged diabatic heating rate (Fig. 1d) shows that the regions of large diabatic heating coincide with the regions of high precipitation and upward mass flux.

In December, January, and February (DJF) over Africa there is a decrease in upward mass flux (Fig. 2a), diabatic heating (Fig. 2c) and precipitation (Fig. 2c) near the equator and an increase south of it, indicating a southward shift of the circulation. These are also regions in which the statistical significance exceeds 90%. However, the trend in precipitation is weaker than the trends in mass flux and diabatic heating, which might be due to changes in land surface [e.g. *Taylor et al.*, 2002]. Furthermore, there are positive

trends in the vertical mass flux, precipitation, and diabatic heating over the Maritime Continent, although, these increases are strongest for mass flux and precipitation. The pattern over the western and central Pacific shows a decrease along the equator and south of it, along with an increase in the mass flux, diabatic heating and precipitation in the south west of that region, implying a southward shift of the circulation. The upward mass flux, diabatic heating and precipitation increase over the northern part of South America and the equatorial Atlantic, and decrease on the eastern and western flanks of these regions, implying a strengthening of the local overturning circulation.

In June, July, and August (JJA), the linear trend in total mass flux shifts southward of the region of upward and downward mass flux over Africa, the Indian Ocean and the Maritime Continent (Fig. 3a). This shift is partly reflected in the diabatic heating trend (Fig. 3b) as well as in the precipitation trend (Fig. 3c), particularly in the western and central Pacific. There is an increase in mass flux and diabatic heating over northern South America and only a slight (less than 0.04 mm d^{-1} over 31 years) increase in precipitation. In the eastern Pacific, roughly between 10 and 20°N and 100 - 130°W , there is an increase in upward mass flux (by about $7 \times 10^{-5} \text{ kg m}^{-2} \text{ s}^{-1}$ over 31 years), a very weak increase in diabatic heating (by about 0.01 - 0.02 K d^{-1} over 31 years) and a distinct increase in precipitation (by about 0.08 mm d^{-1} over 31 years). The decrease in mass flux and diabatic heating south of this region is distinct (about $-8 \times 10^{-5} \text{ kg m}^{-2} \text{ s}^{-1}$ and -0.12 K d^{-1} over 31 years, respectively), but less marked in the precipitation trend (about -0.03 mm d^{-1} over 31 years). In the Atlantic, there is an increase in upward mass flux along about 10°N (by about $5 \times 10^{-5} \text{ kg m}^{-2} \text{ s}^{-1}$ over 31 years) as well as in precipitation (by about 0.08 mm d^{-1}

over 31 years). However, the trend in the diabatic heating is negative in this region (about -0.12 K d^{-1} over 31 years).

4. Local Hadley and Walker circulations

The time-mean local Hadley (Fig. 4) and local Walker (Fig. 5) circulations are defined by the meridional and zonal mass fluxes at 500 hPa and are averaged over the four reanalyses. In both DJF and JJA, the local Hadley circulation (Fig. 4) is characterised by zonally-elongated bands of vertical mass flux, with marked ascent in the tropics and marked subsidence in the subtropics. The ascent is shifted towards the summer hemisphere, whereas the subsidence is more distinct in the winter hemisphere. In the equatorial eastern Pacific, however, there is subsidence along the equator, extending southwards into the extratropics. North of this region, there is strong ascent marking the Inter-Tropical Convergence Zone (ITCZ).

The bands of vertical mass flux comprising the time-mean local Walker circulation are mostly meridionally oriented (Fig. 5). Almost everywhere, the time-mean local Walker circulation is weaker, and its seasonal variation smaller, than the corresponding time-mean local Hadley circulation. In DJF, the time-mean local Walker circulation is most pronounced on the western sides on the Southern Hemisphere continents (Fig. 5a) with ascent over the continents and subsidence over the adjacent oceans. The time-mean local Walker circulation is strongest over the eastern Pacific and South America. Similarly, there are pronounced bands of subsidence over the Atlantic and over the Indian Ocean to the west of Australia. These bands of subsidence are accompanied by ascent on the western side of southern Africa and western Australia. Patterns of alternating ascent and

subsidence lie over the Rocky Mountains, the Middle East and Asia and are most likely a consequence of the underlying orography.

In JJA, the time-mean local Walker circulation (Fig. 5b) is more pronounced in the Northern Hemisphere. Ascent is centered on the Bay of Bengal and to its north, over the western Pacific, and through much of the Americas and the Caribbean. Notable centers of subsidence lie over the eastern Mediterranean Sea, over Somalia and the western Indian Ocean, to the east of the Caspian Sea, and off the west coast of the United States. Strong bands of ascent and subsidence lie along the Andes. These results are in good agreement with those in *Schwendike et al.* [2014], which are based only on the ERAI reanalysis.

The linear trends for the local Hadley and local Walker circulations at 500 hPa show that the regional differences are large and changes in the magnitude of the vertical mass flux range from values between $1\text{-}10\times 10^{-5}\text{ kg m}^{-2}\text{ s}^{-1}$ over 31 years. Additionally, there is no coherent picture around the globe for either the local Hadley (Fig. 6) or the local Walker (Fig. 7) circulation.

In DJF, there is a weakening and a southward shift by about one degree over 31 years of the local Hadley circulation over Africa (Fig. 6a). Over the Indian Ocean a northward shift by about half a degree occurs, whereas over the Maritime Continent the region of the upward mass flux increases more strongly than the downward mass flux leading to an enhancement of the local Hadley circulation. In contrast, over the western and central Pacific the local Hadley circulations are shifted towards the south by about one degree over 31 year. Over South America and the Caribbean as well as in the Atlantic the local Hadley circulations intensify (upward mass flux increases by about $6\times 10^{-5}\text{ kg m}^{-2}\text{ s}^{-1}$ and the downward mass flux decreases by about $-6\times 10^{-5}\text{ kg m}^{-2}\text{ s}^{-1}$ over 31 years). In

JJA, the trends are very similar except that there is a continuous southward shift in the local Hadley circulation all the way from Africa to the western Pacific by about half to one degree over 31 years (Fig. 6b). The local Hadley circulation intensifies in the eastern Pacific, over South America and in the Atlantic with an increase in upward mass flux by about $6 \times 10^{-5} \text{ kg m}^{-2} \text{ s}^{-1}$ and a decrease in downward mass flux by about $-6 \times 10^{-5} \text{ kg m}^{-2} \text{ s}^{-1}$ over 31 years. The trend pattern in the local Hadley circulation (Fig. 6a, b) is very similar to that for the total mass flux (Fig. 2a and Fig. 3a), emphasizing that the local Hadley circulation makes the larger contribution to the total mass flux.

In DJF, the upward mass flux associated with the local Walker circulation over Africa and South America and the downward mass flux on either side intensifies (Fig. 7a). Over parts of the Maritime Continent, along the coast of China and in the eastern Indian Ocean there is a band of increased, i.e. less negative, mass flux as well as decrease in mass flux over India and south of it. Hence, the local Walker circulation in the Indian Ocean as well as in the Atlantic Ocean weakens and shifts to the west. The trend pattern in the Pacific lacks a coherent structure, characterized by a slight weakening (about $-1 \times 10^{-5} \text{ kg m}^{-2} \text{ s}^{-1}$ per 31 years) or no change in the local Walker circulation. The trend pattern in JJA (Fig. 7b) is less pronounced but similar to that in DJF.

A westward shift in the local Walker circulations by on average about $1-2^\circ$ in each ocean basin is evident in Fig. 8. For this analysis we portray the local Walker circulations by the zonal streamfunction ψ_λ . Taking the mean over DJF between 1979 and 2009 reveals three circulations: one in the Pacific Ocean, one in the Indian Ocean, and one in the Atlantic (Fig. 8a). The difference in ψ_λ between 1995-2009 and 1979-1994 shows a decrease from 130° - 180°E and an increase from 80° - 120°E , indicating a shift in the Walker circulation to

the west. There is an increase in ψ_λ in the longitudinal band 120°-70°W, and another in the band 30°W-30°E. Areas of decrease occur between 30°-70°E and 60°-40°W, showing that the local Walker circulations in each basin is shifted westward. This shift to the west is largest in the Pacific and Indian Ocean with about 4-5° over 31 years between 80°E-140°W and 1-2° in the eastern Pacific, but less than that in the Atlantic.

In JJA, the three overturning cells over each ocean basin are present in the meridionally averaged zonal stream function (Fig. 8b), although their position is different to that in DJF. The centre of all circulations is shifted to the west, and the cell in the Indian Ocean is more pronounced than in DJF. The difference between 1995-2009 and 1979-1994 reveals areas of decrease between about 60°E-150°W and 60°-40°W, and areas of increase between 110°-70°W and 30°W-40°E. These changes imply that the local Walker circulation in the Pacific and in the Indian Ocean are shifted to the west. This westward shift is most distinct in the Pacific and over the Maritime Continent with 1-2°. In the other region the local Walker circulation shifts only by about one degree or less. The local Walker circulation in the Atlantic seems to mainly weaken.

5. Meridionally averaged mass flux

The Hovmöller plot for the Hadley circulation at 500 hPa for DJF and JJA, zonally averaged around the whole globe, is shown in Fig. 9. The time on the ordinate ranges from 1979 to 2009 and the latitude is given on the abscissa. During the Southern Hemisphere summer, the strongest mean downward mass flux lies in the Northern Hemisphere subtropics between about 10°N to 35°N, with weaker mean downward mass flux in the Southern Hemisphere, poleward of 30°S (Fig. 9a). The ascending branch of the Hadley circulation straddles the equator, albeit displaced towards the Southern Hemisphere (Fig.

9a). To the extent that the ascending branch can be considered a single region of ascent from, say, 10°N to 20°S , the Hadley circulation comprises a single cell during DJF. This is the conventional view, derived principally from the calculation of a mass-weighted streamfunction [e.g. *Hartmann*, 1994].

During the Northern Hemisphere summer, the Hadley circulation is characterized unequivocally as a single overturning cell (Fig. 9b). There is a band of strong mean upward mass flux in the Northern Hemisphere tropics, accompanied by a band of strong mean downward mass flux in the Southern Hemisphere.

The pattern of the zonally averaged diabatic heating rate (Fig. 9c and d) is very similar to the Hadley circulation (Fig. 9a and b). The vertical mass flux in the meridional plane and the diabatic heating rate are highly correlated in space and time as shown by a pattern correlation coefficient of 0.81 in DJF and 0.91 in JJA.

The linear trend shows that the upward mass flux between the equator and 10°N increases strongly at a rate $1.5 \times 10^{-5} \text{kg m}^{-2} \text{s}^{-1}$ over 31 years in DJF (Fig. 9e). Likewise, the region of downward mass flux during DJF in the Northern Hemisphere decreases (meaning it becomes more negative) at the rate $0.9 \times 10^{-5} \text{kg m}^{-2} \text{s}^{-1}$ over 31 years. Taken together, these results imply a strengthening of the Northern Hemisphere winter cell, in agreement with previous work on the topic (see *Quan et al.* [2004] and the references therein). However, the upward mass flux decreases in the band 10° south of the equator, and increases slightly poleward of that region, indicating a weakening and southward shift of the Southern Hemisphere summer cell.

The upward mass flux in the summer hemisphere in JJA (5°N - 20°N) decreases strongly at a rate of $1.8 \times 10^{-5} \text{kg m}^{-2} \text{s}^{-1}$ over 31 years (Fig. 9f). On either side of this region,

however, the mass flux increases, resulting in a weakening and widening of the Hadley circulation. The magnitude of the downward mass flux between about 5°S - 20°S decreases, i.e. the mass flux becomes less negative, in agreement with the overall weakening of the Hadley circulation.

6. Zonally averaged mass flux

Figure 10 shows the meridional mean of the zonal part of the vertical mass flux at 500 hPa for DJF and JJA from 1979 to 2009, where the meridional average is taken from 35°S to 10°N . This band of latitudes is chosen as the largest zonal vertical mass flux occurs here (see Fig. 5). This field represents the Walker circulation, although the definition is different from those used in past studies. During DJF, the Walker circulation comprises 6 distinct bands of vertical mass flux with alternating sign (or 3 distinct overturning cells; Fig. 10a). The first is a narrow band of mean downward mass flux over the eastern Indian Ocean and southeast Asia (90° - 110°E). This band shows strong variability and a slight weakening over the period (meaning the subsidence is reduced). This weakening can be seen in linear trend in this region which shows an increase in vertical mass flux, i.e. a reduction in downward mass flux (Fig. 10c).

The second is a broad band of mean upward mass flux over the center of the Maritime Continent and the western and central Pacific (120°E - 140°W), while the third is a band of mean downward mass flux over the eastern Pacific and central and north America (140° - 80°W). The fourth band shows mean upward mass flux over South America and the western Atlantic (80° - 40°W). The fifth is a band of mean downward mass flux lying over the eastern Atlantic and Africa (20°W - 15°E). The final band is a mean upward mass flux over the eastern portion of Africa, as well as the western and central Indian Ocean

(15°-90°E). This band is highly variable, with periods of downward mass flux embedded within.

The mass flux increases up to about $1.5 \times 10^{-5} \text{ kg m}^{-2} \text{ s}^{-1}$ over 31 years between (10°-30°E) and (80°-40°W) (Fig. 10c). East of 120°E the mass flux increases and west of 120°E the mass flux decreases, indicating a westward shift by about 4-5° in this region. Overall the changes in vertical mass flux in the Pacific region are small and of varying sign. These results show that over the South America, the Atlantic and Africa, the zonal part of the vertical mass flux has strengthened during DJF in the period 1979 to 2009.

In contrast, the number of distinct bands of vertical mass flux comprising the Walker circulation is less clear during JJA (Fig. 10b) as the vertical mass flux in the band 30°-110°E changes sign. The first band, comprising mean downward mass flux lies from 30°W-15°E. Between 30°W and the Greenwich Meridian the vertical mass flux increases, i.e. it becomes less negative, and it becomes more strongly negative from 10°W -10°E (Fig. 10d). The second is a band of mean upward mass flux from 15°-30°E, which increases particularly towards the end of the period 1979-2009. However, around 30°E the mass flux decreases by about $-1.1 \times 10^{-5} \text{ kg m}^{-2} \text{ s}^{-1}$ over 31 years. The third band is characterized by mean downward mass flux and ranges from 30°-80°E. In this band the mass flux weakens with time (becomes less negative). The fourth band of mean upward mass flux lies from 80°E-160°W, and is made up of two, relatively distinct maxima, one centered over around 100°E and associated with the Asian monsoon, the other centered around 170°E in the western Pacific. The linear trend over this broad band changes sign frequently, but the upward mass flux in the region of the main maxima increases. The fifth is a band of mean downward mass flux from 170°-80°W, which mainly weakens. The sixth is a weak band

of mean upward mass flux from 80° - 50° W, which both strengthens from 80° - 60° W and weakens eastwards of this region.

7. The effect of ENSO on the trends

As ENSO is the largest mode of variability in the tropics it is important to investigate in what way (if any) trends in ENSO affect the calculated trends in the local Hadley and Walker circulations described in the pervious section.

To analyze changes during the two phases of ENSO the differences in the local Hadley and Walker circulations in La Niña and El Niño periods are computed. The El Niño events are defined by a monthly Southern Oscillation Index (SOI) less than -0.9 standard deviation whereas La Niña events are defined by an SOI larger than 0.9 standard deviation. The anomalies for the annual total mass flux (Fig. 11a), GPCP rainfall (Fig. 11b) and diabatic heating (Fig. 11c) show much the same pattern as each other. There are large positive anomalies in the Western and Central Pacific and in the central southern Pacific, emphasising the regions of enhanced convection during El Niño events. Over the Maritime Continent and along the South Pacific Convergence Zone (SPCZ) there is a distinct negative anomaly due to the shift of upward mass flux from the central Pacific to the Maritime continent between El Niño and La Niña periods [e.g. *Rasmusson and Carpenter*, 1982]. Partitioning the vertical mass flux into that associated with the local Hadley circulation (Fig. 11d) and that associated with the local Walker circulation (Fig. 11e) shows that the largest effect of ENSO is on the local Hadley circulation. The anomalies in the local Hadley circulation display a similar pattern to the anomalies in the total mass flux, precipitation and diabatic heating, as El Niño is driven by a tongue of warm sea surface temperatures (SSTs) along the equator. Consequently, the meridional gradients

are larger than the zonal gradients, and, hence, the response in meridional direction is stronger. As a result the local Hadley circulation is larger than the local Walker circulation. Nonetheless, the local Walker circulation strengthens during La Niña and weakens during El Niño. By construction, the sum of the local Hadley circulation and the local Walker circulation is the total mass flux.

To check if there is a trend in the reanalyses related to a trend in ENSO, the monthly SOI time series, as well as its 5-month running mean, and their linear trends are plotted in Fig. 12a. Also plotted in Fig. 12b are the monthly NINO3.4 index and its 5-month running mean. None of the time series has a statistically significant trend. Only the SOI time series show any trends and they are well below the threshold for El Niño and La Niña events.

As an additional test of whether any analyzed trends can be attributed to trends in ENSO two new indices are defined based on the zonal and meridional mass fluxes; these indices are termed M_λ and M_ϕ , respectively. The definition of the M_λ follows the definition of the SOI, which is the standardised anomaly of the Mean Sea Level Pressure difference between Tahiti and Darwin. However, instead of choosing two points, two regions are selected. Region 1 lies over the Maritime Continent (125-135°E, 5°S-5°N) and region 2 is located in the central Pacific (165-155°W, 5°S-5°N). The zonal mass flux at 500 hPa is averaged over both regions, and their difference is taken. M_λ is now defined as the difference between the difference (region 1 - region 2) in every month, and the average value over 31 years of this months.

By analogy with the definition of the NINO3.4 index, a box in the central Pacific (170°E-140°W, 5°S-5°N) is chosen to represent the local Hadley circulation. M_ϕ is defined as the

difference between the monthly average at 500 hPa and the average value over 31 years over that box.

The 5-month running mean of the indices M_λ and M_ϕ for each reanalysis as well as the average over all reanalyses are shown in Fig. 12c and d, respectively. The SOI and the mean M_λ time series are highly correlated, the correlation coefficient being 0.83. The time series from ERAI has the highest correlation with the SOI. The linear trend in the mean time series of M_λ also shows no statistically significant trend. Although the time series from MERRA shows a trend, which can be attributed to the relatively high start and end values of this time series, it is still within one standard deviation. The mean M_ϕ and the NINO3.4 are highly correlated with a correlation coefficient of 0.91. Again the time series from ERAI has the highest individual correlation with a small negative linear trend which is well below the threshold values for ENSO events.

The analysis above shows that there is no significant trend due to ENSO in any of the four reanalyses and that none of the trends analyzed in the previous section are related to changes in ENSO. Moreover, M_λ , which is a measure of the local Walker circulation in the Pacific, shows little trend. Likewise, M_ϕ , which expresses the strength of the mass flux within a box along the equatorial Pacific, shows no change in the last 31 years.

8. Conclusions

In this study a variation of the ψ -vector method developed by *Keyser et al.* [1989] is used to describe local Hadley and local Walker circulations at 500 hPa, based on four reanalyses (ERAI, NCEP2, MERRA and JRA). Further, linear trends for the local Hadley and local Walker circulations are calculated.

Patterns in the trends of the total mass flux, diabatic heating and GPCP precipitation are similar in all seasons. In DJF the trend shows a fairly consistent southward shift in mass flux, diabatic heating and precipitation over Africa, the Maritime Continent and over the northern part of South America. In JJA, the trends in the total mass flux, diabatic heating and precipitation show a southward shift ranging from Africa to the central Pacific. Over northern South America, the mass flux, diabatic heating and precipitation increase. In the Atlantic, the upward mass flux and precipitation increase north of the equator, although the diabatic heating rate decreases.

A key advantage of our decomposition method is that it allows a regional study of changes in Hadley and Walker circulations. We found there is no coherent global picture in the changes in both the local Hadley and local Walker circulation. In addition, there are marked differences from season to season.

In DJF, the local Hadley circulation over Africa, the Maritime Continent, and the western and central Pacific has shifted southwards by about one degree over 31 years and has strengthened by about 1-5% over the South America, the Caribbean and in the Atlantic. In JJA, the local Hadley circulation has shifted southward by about one half to one degree over 31 years in the whole band from Africa to the western Pacific, and has strengthened by about 1-5% over South and middle America and in the eastern Pacific.

The local Walker circulation is weaker than the local Hadley circulation in an absolute sense, but the percentage changes in the local Walker circulation are stronger than the changes in the local Hadley circulation. In both seasons, the local Walker circulations in the Indian Ocean and the Atlantic have weakened, whereas the local Walker circulation has changed little in the Pacific Ocean. The zonal mass flux has increased by about 10-

20% over Africa, the Maritime Continent and South America, and decreased by the about the same amount on either side of it. In only relatively small regions are the linear trends statistically significant at the 90% confidence level, although some of the largest changes (mass flux larger than $4 \times 10^{-5} \text{ kg m}^{-2} \text{ s}^{-1}$ or smaller than $-4 \times 10^{-5} \text{ kg m}^{-2} \text{ s}^{-1}$ per 31 years) occur in these statistically significant regions.

This paper provides a new way to look at the trends in the local Hadley and local Walker circulations and shows that those changes vary greatly around the globe. Furthermore, there is general agreement in the sign and geographical pattern of the trends among the four reanalyses examined here. Although the regions where the trends are statistically significant are small, the results indicate that a more regional treatment of circulation changes is required if we are to understand the effect of climate variability and changes on the major tropical circulation systems. Applying the ψ -vector method provides a useful first step in that direction.

Acknowledgments. This research was supported by the Australian Research Council Grant FS100100081. The data used in this analysis were provided by the European Centre for Medium range Weather Forecasts, the National Centers for Environmental Prediction-Department of Energy, the Japanese Meteorological Agency, and NASA. We would like to thank Neville Nicholls for his helpful suggestions and comments.

References

- Allen, R. J., S. C. Sherwood, J. R. Norris, and C. S. Zender, Recent Northern Hemisphere tropical expansion primarily driven by black carbon and tropospheric ozone, *Nature*, *485*, 350–354, 2012.
- Bayr, T., D. Dommenges, T. Martin, and S. B. Power, The eastward shift of the Walker circulation in response to global warming and its relationship to ENSO variability, *Clim. Dyn.*, pp. DOI 10.1007/s00382-014-2091-y, 2014.
- Chen, J., B. Carlson, and A. Genio, Evidence for strengthening of the tropical general circulation in the 1990s, *Science*, *296*, 838–841, 2002.
- Davis, S. M., and T. Birner, Seasonal to multi-decadal variability of the width of the tropical belt, *J. Geophys. Res.*, *118*, 7773–7787, 2013.
- Davis, S. M., and K. H. Rosenlof, A multi-diagnostic intercomparison of tropical width time series using reanalyses and satellite observations, *J. Clim.*, *25*, 1061–1078, 2012.
- Dee, D. P., et al., The ERA-Interim reanalysis: configuration and performance of the data assimilation system, *Q. J. R. Meteorol. Soc.*, *137*, 553–597, 2011.
- Deser, C., and A. S. Phillips, Atmospheric circulation trends, 1950-2000: The relative roles of sea surface temperature forcing and direct atmospheric radiative forcing, *J.*

Clim., 22, 396–413, 2009.

DiNezio, P. N., G. A. Vecchi, and A. C. Clement, Detectability of changes in the Walker circulation in response to global warming, *J. Clim.*, 26, 4038–4048, 2013.

Fu, Q., and P. Lin, Poleward shift of subtropical jets inferred from satellite-observed lower stratospheric temperatures, *J. Climate*, 24, 5597–5603, 2011.

Fu, Q., C. M. Johanson, J. M. Wallace, and T. Reichler, Enhanced mid-latitude tropospheric warming in satellite measurements, *Science*, 312, 1179, 2006.

Gastineau, G., H. Le Treut, and L. Li, Hadley circulation changes under global warming conditions indicated by coupled climate models, *Tellus*, 60, 863–884, 2008.

Gastineau, G., L. Li, and H. Le Treut, The Hadley and Walker circulation changes in global warming conditions described by idealized atmospheric simulations, *J. Climate*, 22, 3993–4013, 2009.

Gedney, N., and P. J. Valdes, The effect of Amazonian deforestation on the Northern Hemisphere circulation and climate, *Geophys. Res. Lett.*, 27, 3053–3056, 2000.

Goswami, B. N., V. Krisnamurthy, and H. Annamalai, A broadscale index for the interannual variability of the Indian summer monsoon, *Q. J. R. Meteorol. Soc.*, 125, 611–633, 1999.

Hartmann, D., *Global Physical Climatology*, 411 pp., Academic Press, 1994.

Held, I. M., and B. J. Soden, Robust responses of the hydrological cycle to global warming, *J. Clim.*, 19, 5686–5699, 2006.

Hu, Y., and Q. Fu, Observed poleward expansion of the Hadley circulation since 1979, *Atmos. Chem. Phys.*, 7, 5229–5236, 2007.

- Hu, Y., and Q. Fu, Poleward expansion of the Hadley circulation in CMIP5 simulations, *Adv. Atmos. Sci.*, *30*, 790–795, 2013.
- Johanson, C., and Q. Fu, Hadley cell widening: Model simulations versus observations, *J. Climate*, *22*, 2713–2725, 2009.
- Julian, P. R., and R. M. Chervin, A study of the Southern Oscillation and the Walker circulation phenomenon, *Mon. Wea. Rev.*, *106*, 1433–1451, 1978.
- Keyser, D., B. D. Schmidt, and D. G. Duffy, A technique for representing three-dimensional vertical circulations in baroclinic disturbance, *Mon. Wea. Rev.*, *117*, 2463–2494, 1989.
- Kistler, R., et al., The NCEP-NCAR 50-year reanalysis: Monthly means CD-ROM and documentation, *Bull. Am. Meteorol. Soc.*, *82*, 247–267, 2001.
- Liu, J., M. Song, and X. Ren, Changes in the strength and width of the Hadley circulation since 1871, *Clim. Past*, *8*, 1169–1175, 2012.
- Lu, J., G. A. Vecchi, and T. Reichler, Expansion of the Hadley cell under global warming, *Geophys. Res. Lett.*, *34*, doi: 10.1029/2006GL028443, 2007.
- Lucas, C., B. Timbal, and H. Nguyen, The expanding tropics: A critical assessment of the observational and modeling studies, *Wiley Interdiscip. Rev.: Climatic Change*, *5*, 89–112, 2013.
- Nguyen, H., A. Evans, C. Lucas, I. Smith, and B. Timbal, The Hadley circulation in reanalyses: Climatology, variability, and changes, *J. Clim.*, *26*, 3357–3376, 2013.
- Onogi, K., et al., The JRA-25 reanalysis, *J. Meteor. Soc. Japan*, *85*, 369–432, 2007.
- Power, S., and I. Smith, Weakening of the Walker Circulation and apparent dominance of El-Nino both reach record levels, but has ENSO really changed?, *Geophys. Res. Lett.*,

34, doi:10.1029/2007GL030,854, 2007.

Quan, X., H. Diaz, and M. Hoerling, Changes in the Tropical Hadley cell since 1950, in *Chapter 3, The Hadley Circulation: Present, Past and Future*, edited by H. F. Diaz and R. S. Bradley, pp. 85–120, Kluwer Academic Publishers, 2004.

Quan, X.-W., M. P. Hoerling, J. Perlwitz, H. F. Diaz, and T. Xu, How fast are the tropics expanding?, *J. Climate*, 27, 1999–2013, 2014.

Rasmusson, E. M., and T. H. Carpenter, Variations in tropical sea surface temperature and surface wind fields associated with the Southern Oscillation/El Niño, *Mon. Wea. Rev.*, 110, 354–384, 1982.

Rienecker, M. M., et al., MERRA: NASA’s modern-era retrospective analysis for research and applications, *J. Climate*, 24, 3624–3648, 2011.

Schwendike, J., P. Govekar, M. J. Reeder, R. Wardle, G. J. Berry, and C. Jakob, Local Partitioning of the overturning circulation in the tropics and the connection to the Hadley and Walker circulations, *J. Geophys. Res. Atmos.*, 119, 2014.

Seidel, D., and W. Randel, Recent widening of the tropical belt: Evidence from tropopause observations, *J. Geophys. Res.*, 112, doi:10.1029/2007JD008,861, 2007.

Seidel, D., Q. Fu, W. Randel, and T. Reichler, Widening of the tropical belt in a changing climate, *Nat. Geosci.*, 1, 21–24, 2008.

Simmons, A., S. Uppala, D. Dee, and S. Kobayashi, New ECMWF reanalysis products from 1989 onwards, *ECMWF Newsletter*, 110, 26–35, 2011.

Stachnik, J. P., and C. Schumacher, A comparison of the Hadley circulation in modern reanalyses, *J. Geophys. Res.*, 116, doi:10.1029/2011JD016,677, 2011.

- Tanaka, H., N. Ishizaki, and A. Kitoh, Trend and interannual variability of Walker, monsoon and Hadley circulations defined by velocity potential in the upper troposphere, *Tellus*, *56*, 250–269, 2004.
- Taylor, C. M., E. F. Lambin, N. Stephenne, R. J. Harding, and R. J. Essery, The influence of land use change on climate in the Sahel, *J. Climate*, *15*, 3615–3629, 2002.
- Tokinaga, H., S.-P. Xie, C. Deser, Y. Kosaka, and Y. M. Okumura, Slowdown of the Walker circulation driven by tropical Indo-Pacific warming, *Nature*, *491*, 439–443, 2012.
- Vecchi, G., and B. Soden, Increased tropical Atlantic wind shear in model projections of global warming, *Geophys. Res. Lett.*, *34*, doi:10.1029/2006GL028,905, 2007.
- Vecchi, G., B. Soden, A. Wittenberg, I. Held, A. Leetmaa, and M. Harrison, Weakening of tropical Pacific atmospheric circulation due to anthropogenic forcing, *Nature*, *441*, 73–76, 2006.

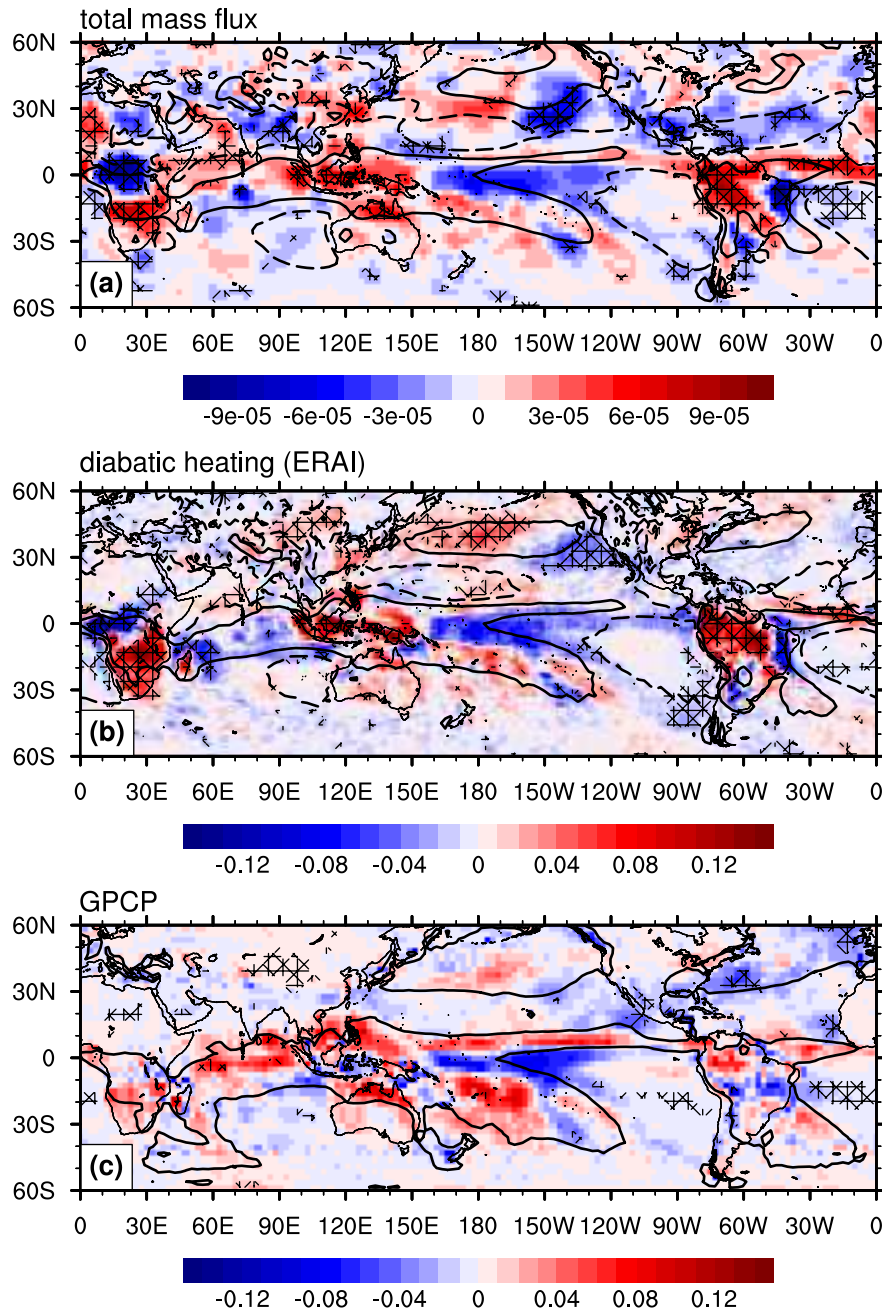


Figure 2. (a) The linear trend between 1979 and 2009 of the total mass flux ($\text{kg m}^{-2} \text{ s}^{-1}$ per 31 years) at 500 hPa based on the average of the mass flux in ERAI, NCEP2, MERRA, and JRA reanalyses for the season DJF. The contours of mean total mass flux of $\pm 0.001 \text{ kg m}^{-2} \text{ s}^{-1}$ illustrate the regions of ascent and descent. (b) The linear trend of the diabatic heating (K d^{-1} per 31 years) at 500 hPa between 1979 and 2009 based on the ERAI reanalysis. The mean diabatic heating of $\pm 1.0 \text{ K d}^{-1}$ is show in contours. (c) The linear trend between 1979 and 2009 of the GPCP precipitation (mm d^{-1} per 31 years) for DJF and JJA. The mean precipitation of 3.0 mm d^{-1} is show in contours. The cross hatching in all plots highlights the regions where the linear trend has a statistical significance of 90%.

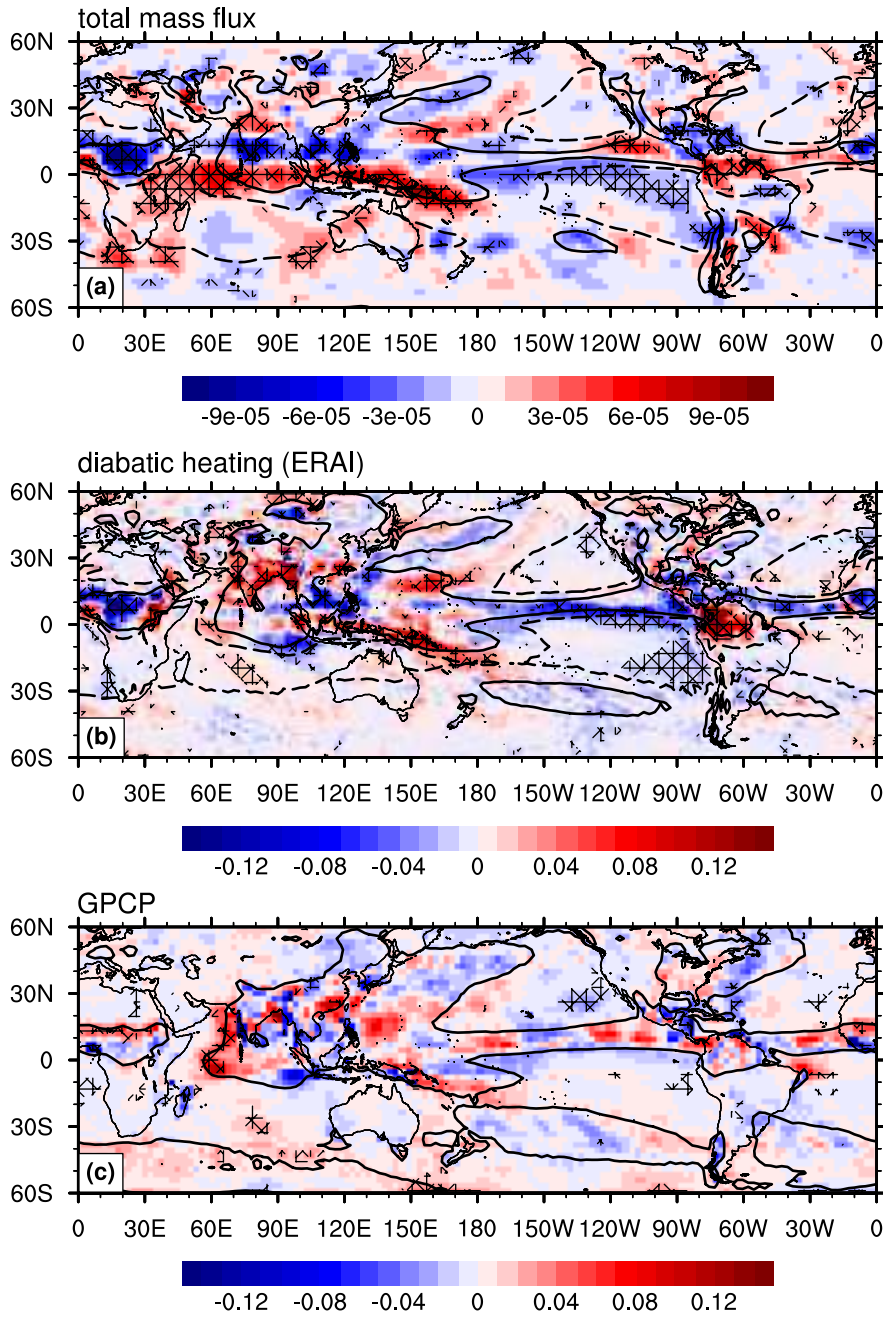


Figure 3. The same as Fig. 2, but for JJA.

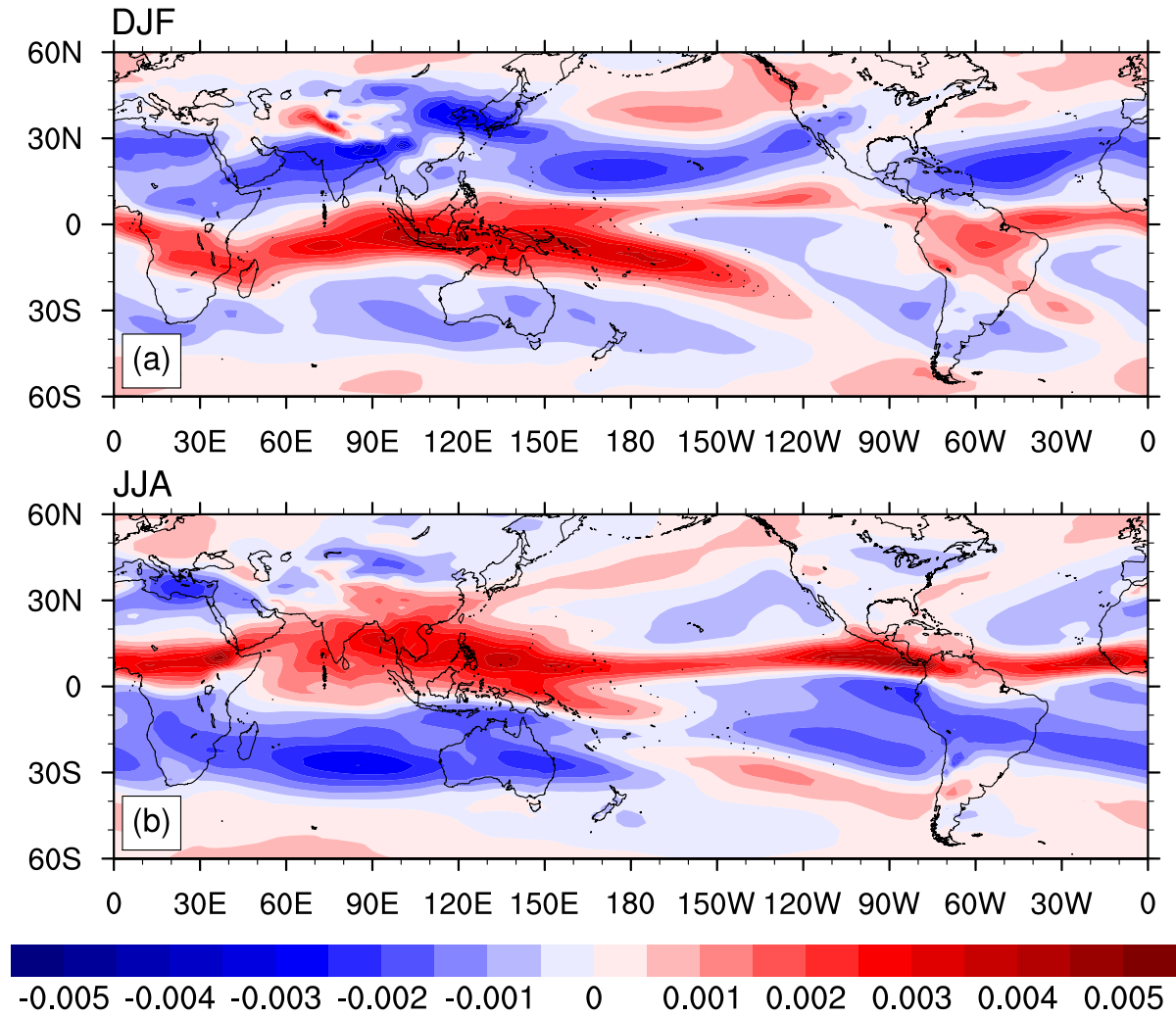


Figure 4. The local Hadley circulation. The meridional mass flux ($\text{kg m}^{-2} \text{s}^{-1}$) for the seasons (a) DJF and (b) JJA is shown in shadings of red (ascent) and blue (descent) at 500 hPa and are averaged over ERAI, NCEP2, MERRA, and JRA reanalyses (1979-2009).

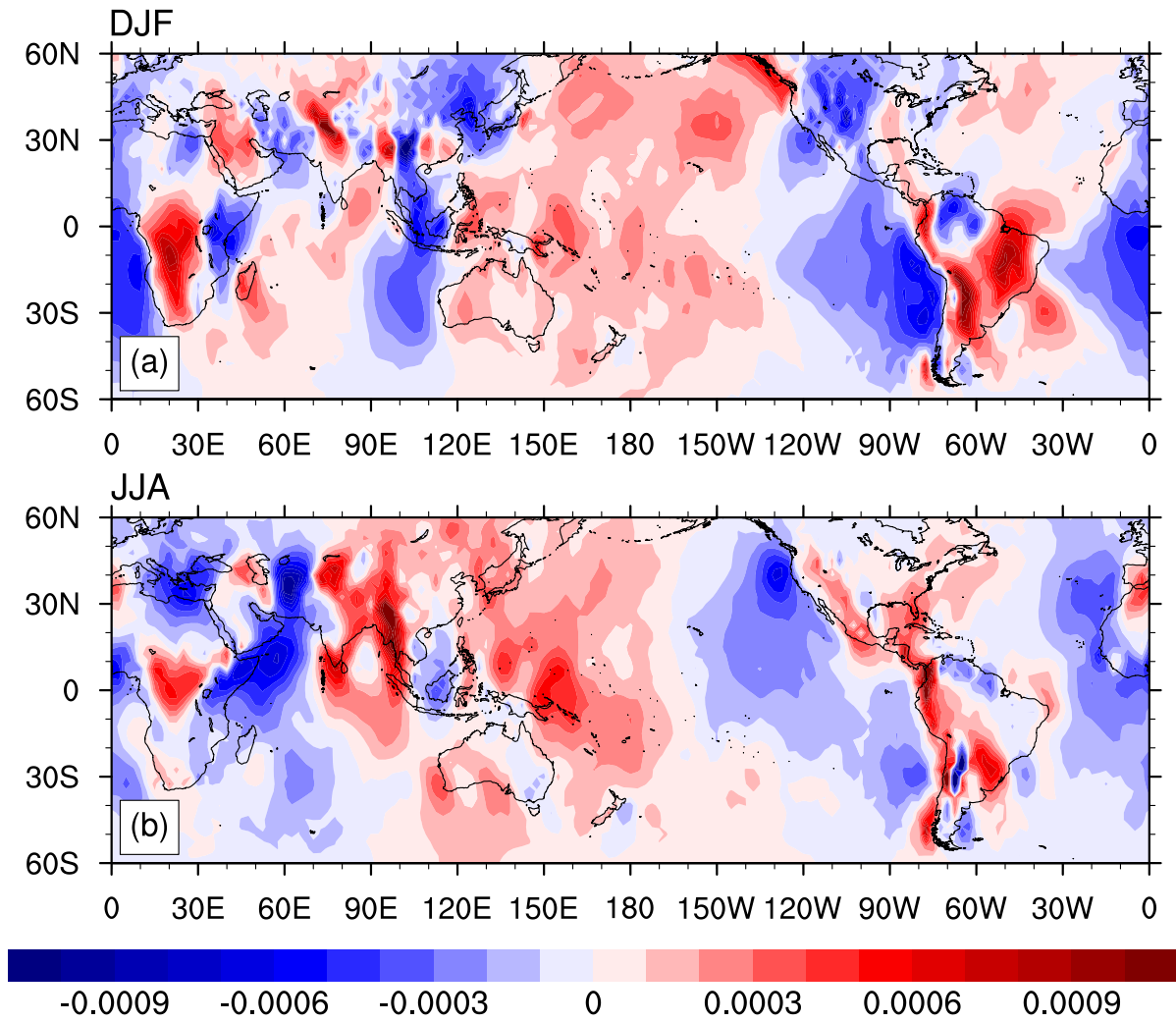


Figure 5. The local Walker circulation. The zonal mass flux ($\text{kg m}^{-2} \text{s}^{-1}$) for the seasons (a) DJF and (b) JJA are shown in shadings of red (ascent) and blue (descent) at 500 hPa and are averaged over ERAI, NCEP2, MERRA, and JRA reanalyses (1979-2009).

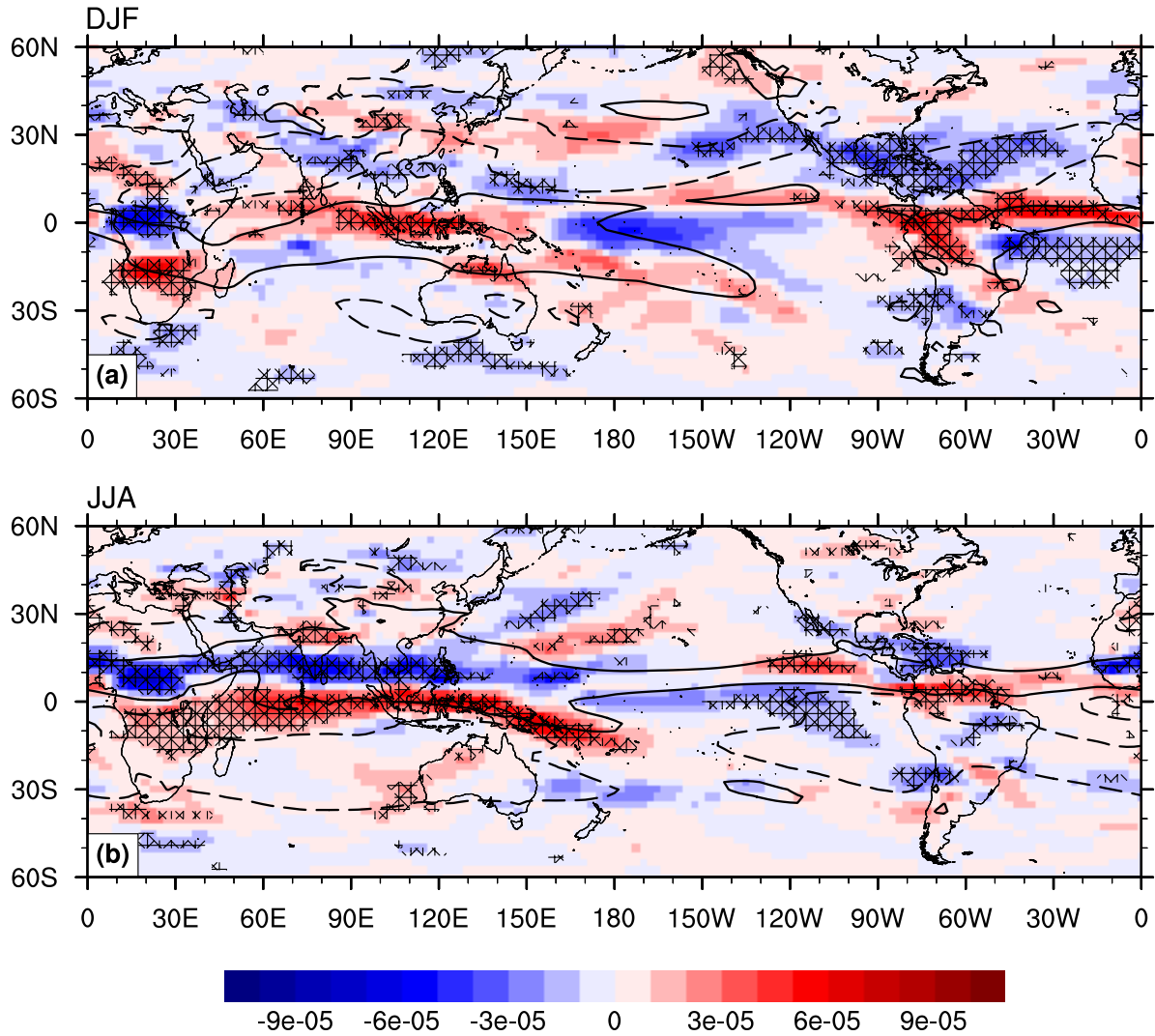


Figure 6. The linear trend between 1979 and 2009 at 500 hPa for the local Hadley circulation based on the average of meridional and zonal mass flux, respectively, in the ERAI, NCEP2, MERRA, and JRA reanalyses. The trend in the mean meridional mass flux ($\text{kg m}^{-2} \text{s}^{-1}$ per 31 years) for the seasons (a) DJF and (b) JJA is shown in shadings of red (increase) and blue (decrease). The contours of the mean meridional mass flux of $\pm 0.001 \text{ kg m}^{-2} \text{s}^{-1}$ illustrate the regions of ascent and descent. The cross hatching highlights the regions where the linear trend has a statistical significance of 90%.

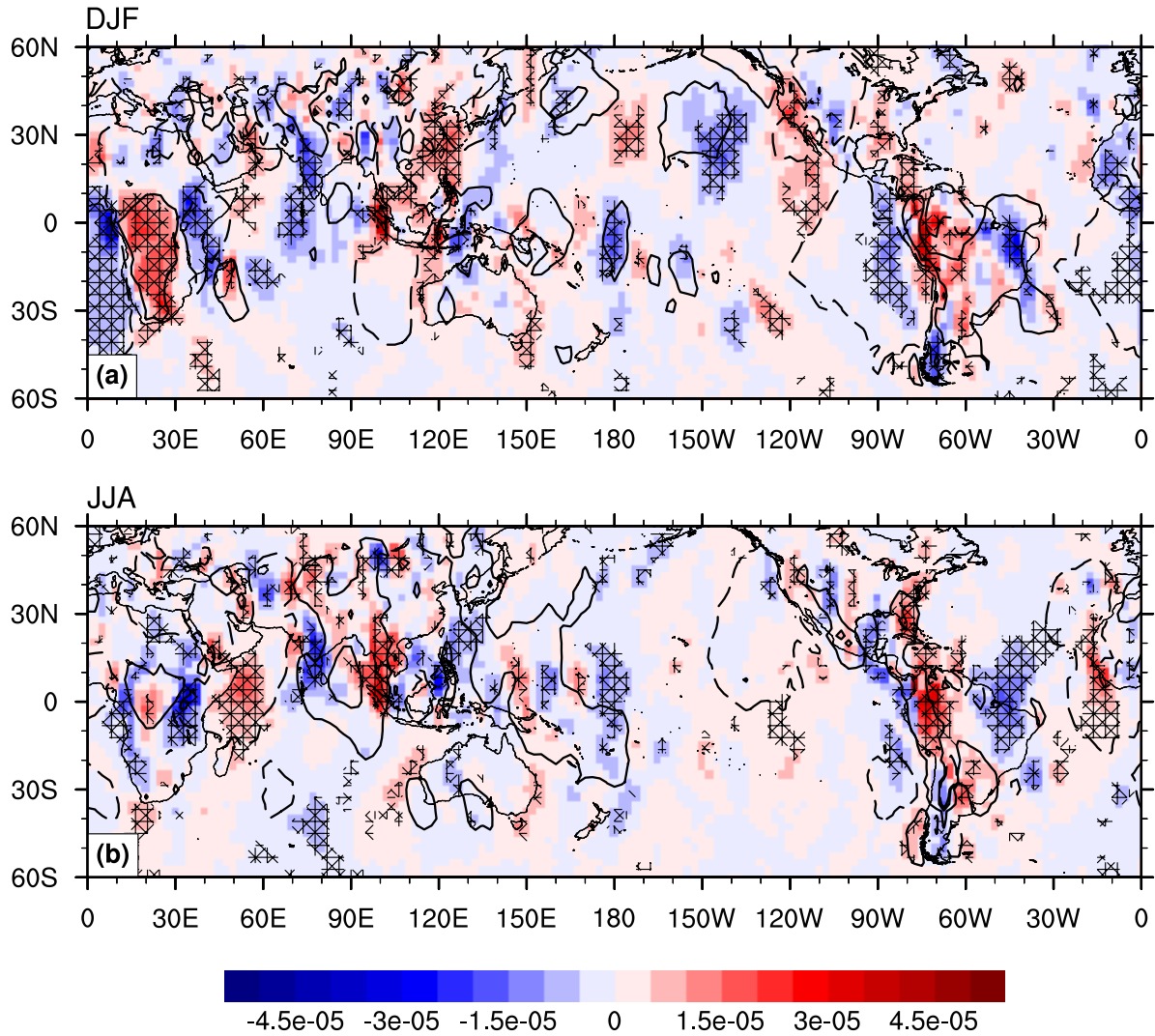


Figure 7. The linear trend between 1979 and 2009 at 500 hPa for the local Walker circulation based on the average the zonal mass flux in the ERAI, NCEP2, MERRA, and JRA reanalyses. The trend in the mean zonal mass flux ($\text{kg m}^{-2} \text{s}^{-1}$ per 31 years) for the seasons DJF and JJA is shown in (a) and (c), respectively. The contours of mean zonal mass flux of $\pm 0.002 \text{ kg m}^{-2} \text{s}^{-1}$ illustrate the regions of ascent and descent. The cross hatching highlights the regions where the linear trend has a statistical significance of 90%.

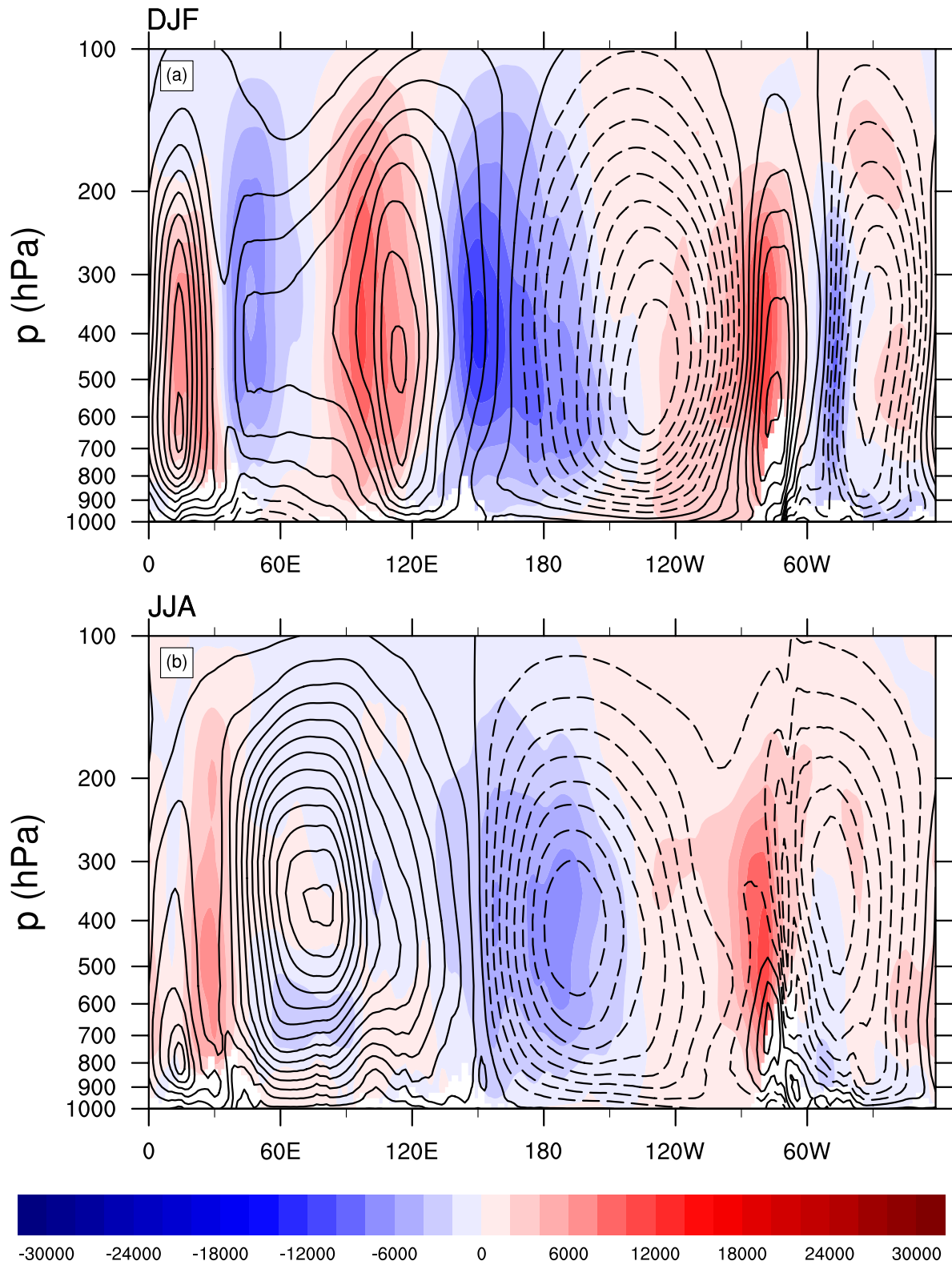


Figure 8. The difference of the zonal streamfunction ψ_λ between (1995-2009) and (1979-1994) for the seasons (a) DJF and (b) JJA shaded, and the position of the mean zonal streamfunction over 1979-2009 in contours. Both are averaged between 35°S and

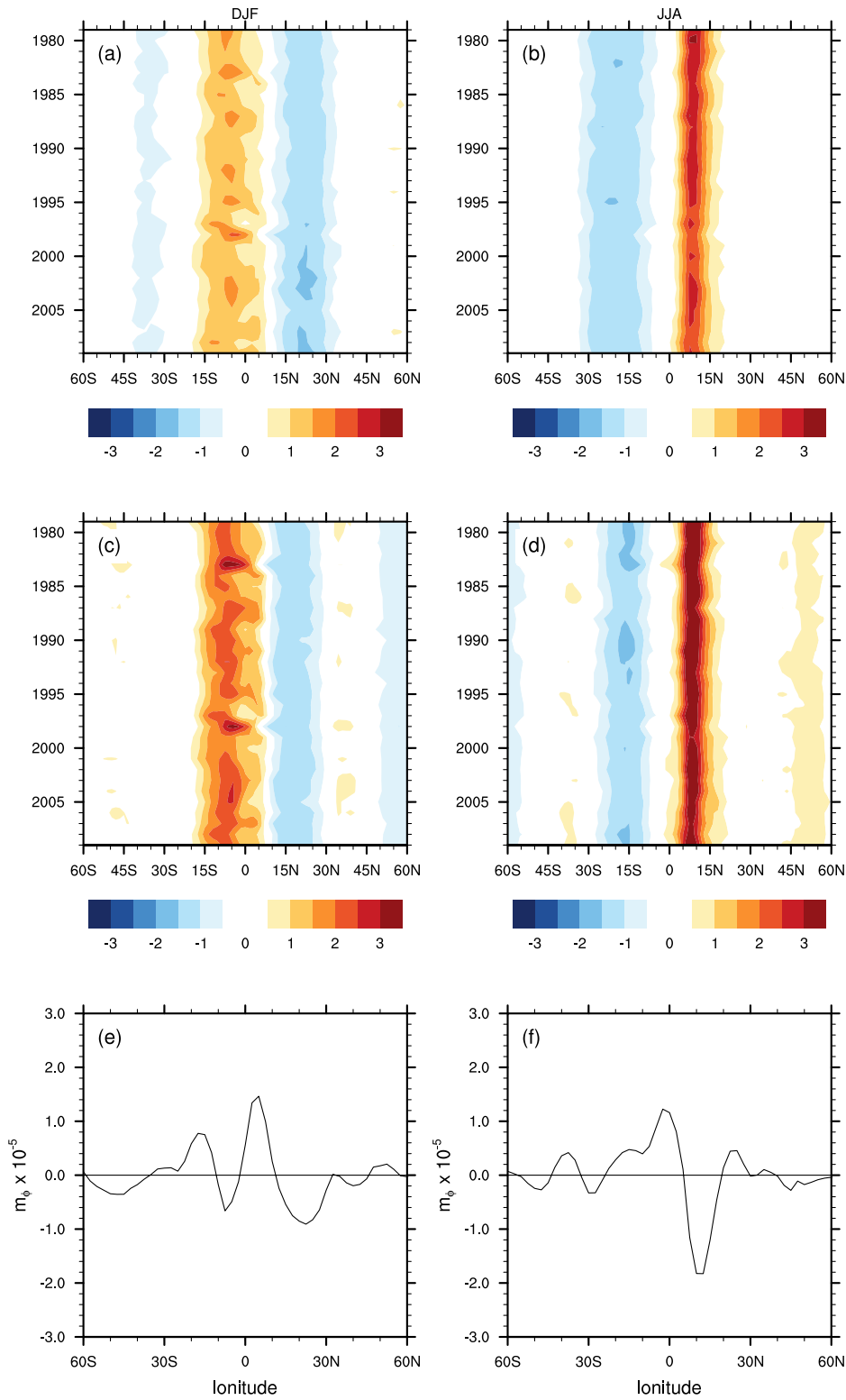


Figure 9. (a, b) The meridional vertical mass flux at 500 hPa averaged over ERAI, NCEP2, MERRA, and JRA reanalyses between 1979 and 2009 ($\times 10^{-3} \text{ kg m}^{-2} \text{ s}^{-1}$) for the seasons DJF and JJA. (c, d) The diabatic heating (K d^{-1}) based on ERAI. (e, f) The averaged trend in meridional mass flux ($\times 10^{-5} \text{ kg m}^{-2} \text{ s}^{-1}$ over 31 years).

DRAFT

September 30, 2014, 3:15pm

DRAFT

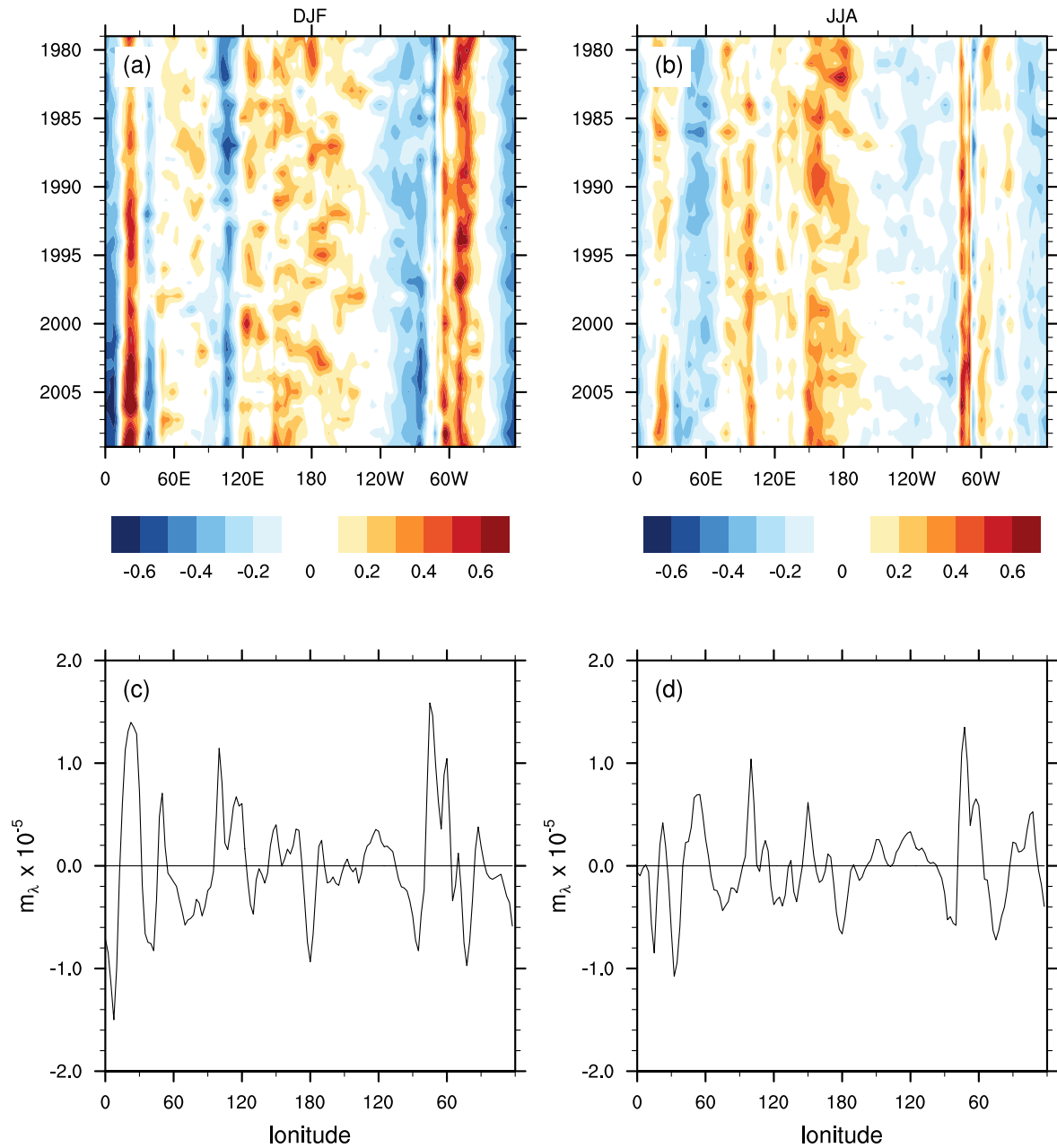


Figure 10. The zonal vertical mass flux at 500 hPa averaged over ERAI, NCEP2, MERRA, and JRA reanalyses between 1979 and 2009 ($\times 10^{-3} \text{ kg m}^{-2} \text{ s}^{-1}$) for the seasons (a) DJF and (b) JJA. (c, d) The averaged trend in zonal mass flux ($\times 10^{-5} \text{ kg m}^{-2} \text{ s}^{-1}$ over 31 years).

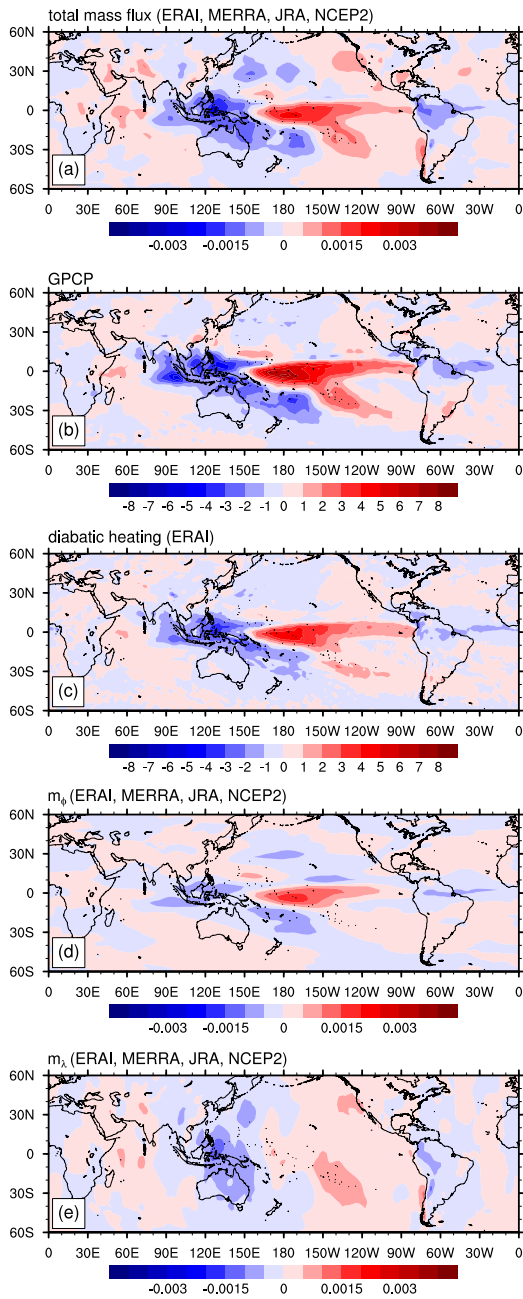


Figure 11. Differences between El Niño and La Niña. (a) The annual average of the total mass flux ($\text{kg m}^{-2} \text{s}^{-1}$) at 500 hPa averaged over ERA1, NCEP2, MERRA and JRA reanalyses (1979 - 2009). (b) The annual average of the GPCP precipitation (mm d^{-1}) between 1979 and 2009. (c) The annual average of the diabatic heating (K d^{-1}) calculated as a residual from potential temperature budget based on the ERA1 reanalysis. (d) The annual average of the mass flux in meridional dircetion ($\text{kg m}^{-2} \text{s}^{-1}$) at 500 hPa averaged over ERA1, NCEP2, MERRA and JRA reanalyses (1979 - 2009). (e) The annual average of the mass flux in zonal dircetion ($\text{kg m}^{-2} \text{s}^{-1}$) at 500 hPa averaged over ERA1, NCEP2, MERRA and JRA reanalyses (1979 - 2009).

D R A F T

September 30, 2014, 3:15pm

D R A F T

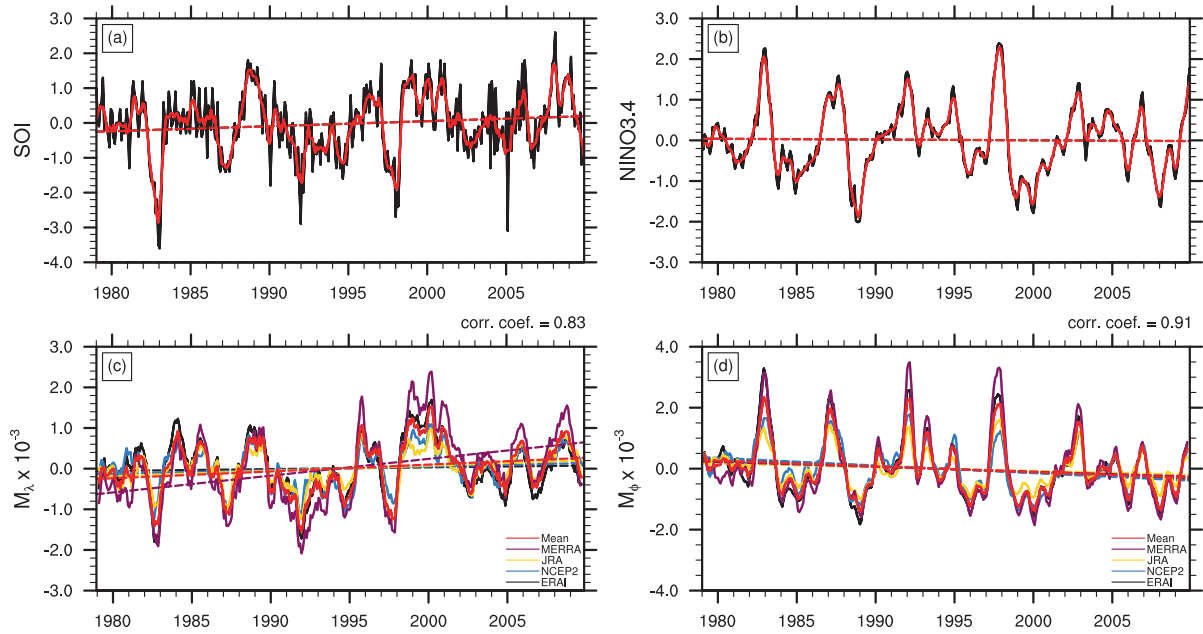


Figure 12. (a) Time series for the monthly SOI (black) and the 5-months running mean of the SOI (red). (b) Time series for the monthly NINO3.4 (black) and the 5-months running mean of the NINO3.4 index (red). (c) Time series of the 5-months running mean of the index M_λ for ERAI (black), NCEP2 (blue), JRA (yellow), MERRA (purple) and the average over all four reanalyses (MEAN in red). The correlation coefficient between the 5-months running mean of the SOI and the 5-months running mean of the mean of the M_λ is shown in the top right corner. (d) Time series of the 5-months running mean of the new index M_ϕ for ERAI (black), NCEP2 (blue), JRA (yellow), MERRA (purple) and the average over all four reanalyses (MEAN in red). The correlation coefficient between the 5-months running mean of the NINO3.4 and the 5-months running mean of the mean M_ϕ , averaged over the 4 reanalyses, is shown in the top right corner. Details on the new indices M_λ and M_ϕ can be found in Section 7.